Available online at www.sciencedirect.com
SCIENCE DIRECT®
ELSEVIER
Nuclear Instruments and Methods in Physics Research A 531 (2004) 435–444
NUCLEAR INSTRUMENTS & METHODS IN PHYSICS RESEARCH Section A
www.elsevier.com/locate/nima

Transition radiation detectors for energy measurements at high Lorentz factors

S.P. Wakely[a,*], S. Plewnia[b], D. Müller[a], J.R. Hörandel[b], F. Gahbauer[a]

[a] *Enrico Fermi Institute, University of Chicago, Chicago, IL 60637, USA*
[b] *Institute for Experimental Nuclear Physics, University of Karlsruhe, P.O. 3640, 76021 Karlsruhe, Germany*

Received 5 December 2003; received in revised form 1 April 2004; accepted 24 April 2004

Available online 25 June 2004

Abstract

The characteristic dependence of the intensity of transition radiation (TR) on the Lorentz factor $\gamma = E/mc^2$ of a primary particle is key to a number of practical applications. In particular, one may use TR detectors for energy measurements of heavy cosmic-ray nuclei in a region where alternate techniques are difficult to apply. However, a serious constraint can be the saturation of the TR yield at high γ-values. We investigate how the onset of saturation can be pushed to as high a Lorentz factor as possible. We then describe the results of test measurements at CERN, which demonstrate the possibility of practical configurations for measurements over the Lorentz factor range of a few hundred to about 10^5.

PACS: 29.40.Cs; 95.55.Vj

Keywords: Transition radiation; TRD; Measurement techniques; Cosmic rays

1. Introduction

Transition radiation (TR) [1] is one of the less familiar electromagnetic radiation processes, as its intensity is usually small and it is easily observable only if the generating particles are highly relativistic. However, the characteristic dependence of TR on the Lorentz factor, $\gamma = E/mc^2$, of a particle lends itself to a number of interesting applications.

TR may be emitted when a charged particle traverses the interface between two different dielectrics. For highly relativistic particles, the photons appear in the X-ray region. However, for particles with unit charge, the probability of emitting a photon is small, of the order $\alpha \approx \frac{1}{137}$ per interface. In order to enhance the intensity, practical instruments use "radiators" of inhomogeneous materials providing hundreds of interfaces.

Practical TR detectors (TRDs) often consist of sandwich combinations of several radiators and detectors. Typically, the detectors are gaseous

*Corresponding author.
E-mail address: wakely@uchicago.edu (S.P. Wakely).

0168-9002/$ - see front matter © 2004 Elsevier B.V. All rights reserved.
doi:10.1016/j.nima.2004.04.245

devices containing xenon for optimum X-ray absorption. The TR photons are emitted at a very small angle $\theta \sim 1/\gamma$ with respect to the direction of the particle trajectory. Therefore, the detector will generate a signal due to TR X-rays which is superimposed on the signal due to the ionization energy loss of the particle, unless special measures are taken, such as magnetically deflecting the particle from the detector. A review of a variety of configurations used can be found in Ref. [2].

There are two typical applications of TRDs. First, one may use a TRD as a threshold device to provide discrimination between particles of some given energy or momentum but with different rest masses, and therefore different Lorentz factors. For instance, one may accomplish discrimination between protons and electrons, pions and electrons, or pions and protons, etc., simply by investigating whether the particle is accompanied by TR photons or not. This application is employed not only in experiments at accelerators, but also in several cosmic-ray detectors. For threshold TRDs, it is desirable that the transition from no TR signal to saturated TR signal occurs over a relatively small range of Lorentz factor. The threshold value of γ may be varied by appropriately choosing the parameters of radiators and detectors; Lorentz factor thresholds from several hundred to several thousand are possible.

The second application of TRDs is more demanding: here, one seeks to measure the radiation intensity in order to obtain an estimate of γ, i.e., of the particle's energy, when the mass is known. It is very difficult to perform such a measurement for singly-charged particles on an event-by-event basis, because of the large statistical fluctuations in both the ionization loss signal and the superimposed TR signal. However, this situation becomes qualitatively different when the primary particle is a nucleus with an electric charge $Z > 1$. Since both the ionization signal and the TR intensity scale with Z^2, the relative magnitude of fluctuations decreases with $1/Z$, and the measurement precision improves significantly with increasing Z. For example, consider a proton (or pion, or electron) with $\gamma \sim 1000$ that produces, on average, one single detectable photon with an average energy of 10 keV. Obviously, the signals from this particle will undergo large Poisson fluctuations, with no TR signal being observed at all for 37% of the events. On the other hand, if the particle is an iron nucleus ($Z = 26$), again at $\gamma \sim 1000$, one would detect, on average, 676 photons, each at 10 keV. The distribution of X-ray signals would then become a rather narrow Gaussian with a width of a few percent, around an average of 6.76 MeV.

Highly relativistic, high-Z particles are rarely encountered in accelerator experiments, but they are, of course, found in the galactic cosmic rays. Hence, TRDs have become attractive devices for measurements of the energy of cosmic-ray nuclei. Contrary to the threshold TRD case, in this application one wishes to obtain a γ-dependent signal over a large range of Lorentz factors, i.e., one desires a gradual transition from zero TR signal to a saturated TR signal [3]. Obtaining such a large dynamic range in γ-values requires that the parameters of the TRD be carefully "tuned". In the past, energy measurements with TRDs have been restricted to below $\gamma \sim 10^4$. However, a key problem in cosmic ray astrophysics is the understanding of the cosmic ray composition in the region of the spectral "knee" around 10^{15} eV per particle [4]. If TRDs are to be used for measurements in this region, their response should not saturate until Lorentz factors of $\gamma \sim 10^5$ are reached. In the following, we discuss the design of practical TRDs for energy measurements over the entire range $\gamma \sim 500$–10^5.

2. Basic properties of TR

A description of the properties and theory of TR is available in several detailed publications [5–9]. For the purpose of this paper, we will simply review and discuss some of the relevant results.

2.1. Frequency spectrum

When a particle of charge Z and Lorentz factor γ traverses a single boundary between two media of differing dielectric constant, the differential energy spectrum of TR in the X-ray

region is

$$\frac{\mathrm{d}^2 W_0}{\mathrm{d}\omega\,\mathrm{d}\theta} = \frac{2\alpha\hbar\theta^3 Z^2}{\pi} \left| \frac{1}{\gamma^{-2}+\theta^2+\xi_1^2} - \frac{1}{\gamma^{-2}+\theta^2+\xi_2^2} \right|^2 \quad (1)$$

where θ is the emission angle of the photons with respect to the particle trajectory, ω the frequency of the emitted radiation, α the fine structure constant, and $\xi_i \equiv \omega_i/\omega$ the ratio of a material's plasma frequency to the emitted photon frequency, such that the dielectric constant $\varepsilon_i \approx 1 - \xi_i^2$. This expression is valid in the relativistic ($\gamma \gg 1$), small-angle ($\theta \ll 1$), high-frequency ($\omega \gg \omega_i$) limit.

The emission of the photons is sharply peaked in the forward direction, near $\theta \sim 1/\gamma$. Integrating Eq. (1) over angles and frequencies gives the total radiation yield:

$$W_0 = \frac{\alpha\hbar Z^2}{3} \frac{(\omega_1-\omega_2)^2}{\omega_1+\omega_2}\gamma. \quad (2)$$

The linear increase in total yield comes primarily from a hardening of the emitted X-rays, rather than from an increase in the overall photon multiplicity.

For a radiator consisting of multiple foils, the frequency distribution exhibits a characteristic oscillatory nature which is caused by interference effects between the emission amplitudes of all the media boundaries in the radiator. For an N-foil regular stack with constant spacings l_2 and foil thickness l_1, one obtains

$$\frac{\mathrm{d}^2 W_N}{\mathrm{d}\omega\,\mathrm{d}\theta} = \frac{\mathrm{d}^2 W_0}{\mathrm{d}\omega\,\mathrm{d}\theta} 4\sin^2\left(\frac{l_1}{z_1}\right) \frac{\sin^2[N(l_1/z_1+l_2/z_2)]}{\sin^2(l_1/z_1+l_2/z_2)}. \quad (3)$$

Here, $\mathrm{d}^2 W_0/\mathrm{d}\omega\,\mathrm{d}\theta$ is the single-interface emission spectrum, given by Eq. (1), and one assumes reabsorption in the radiator to be negligible. The characteristic length scales z_i are called "formation zones". They may be thought of as roughly the distance required for the electromagnetic field of a moving particle to reach a new equilibrium state in the medium it has just entered [9]. The formation zones are defined as

$$z_i \equiv \frac{4c}{\omega} \frac{1}{\gamma^{-2}+\theta^2+\xi_i^2}. \quad (4)$$

Eq. (3) shows that the yield of the radiator stack is determined by the ratios of the foil and gap thicknesses to their formation zones. For $l_1 \ll z_1$, the first $\sin^2$ term drops to zero, effectively suppressing the yield. However, when both l_1 and l_2 are larger than z_1 and z_2, the total integrated yield from a stack of foils will approach $2N$ times the yield from a single interface [8].

Fig. 1 shows the approximate differential energy spectrum ($\mathrm{d}W_N/\mathrm{d}\omega$), obtained by integrating Eq. (3) over all angles. It is normalized by the number of interfaces and compared with the single interface spectrum (Eq. (1)). The broad, final maximum of the multifoil spectrum contains a major portion of the total emission and is located

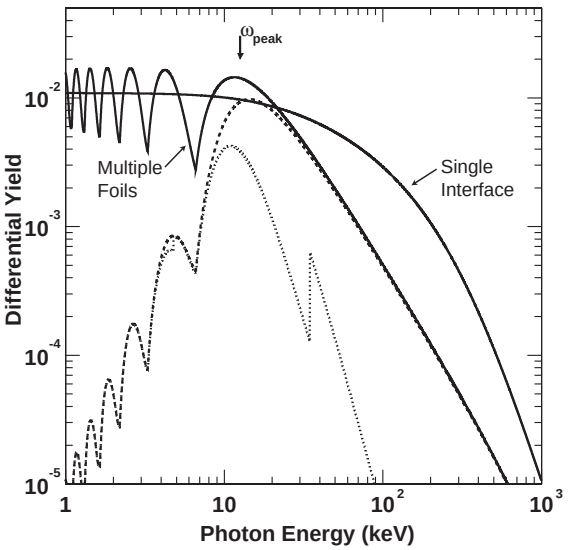

Fig. 1. Differential TR yield ($\mathrm{d}W/\mathrm{d}\omega$) versus Lorentz factor for several configurations. Shown are the single-interface (smooth line) and approximate multi-foil (oscillating line) energy spectra, as well as the multi-foil spectrum modified by self-absorption processes in the foil (dashed line). The dotted line shows the yield which would be captured in a single 1 cm thick layer of xenon. The characteristic peak emission energy ω_{peak} is also indicated. All spectra are normalized to a single-interface yield. The relevant parameters are $\gamma = 2\times10^4$, $l_1 = 35$ μm, $l_2 = 1000$ μm, $\omega_1 = 21.2$ eV, and $\omega_2 = 0.75$ eV.

around a characteristic peak energy [8]:

$$\omega_{\text{peak}} \approx \omega_1^2 l_1 / 2\pi c. \quad (5)$$

2.2. Saturation

The total yield of TR from a stack of foils does not increase indefinitely with γ. Instead, saturation effects begin to limit additional photon production as the Lorentz factor rises. The formation zones z_1 and z_2 have a strong dependence on the Lorentz factor of the particle, and will eventually become larger than l_1 and/or l_2, respectively. This will limit the total TR emission to reaching a plateau value. The Lorentz factor at which these effects begin to become appreciable in a multifoil radiator has been predicted [9,10] to be about

$$\gamma_{\text{sat}} \approx 0.6\omega_1 \sqrt{l_1 l_2}/c. \quad (6)$$

2.3. Irregular radiators

For practical reasons, one often uses radiators that are composed of foams or fibers rather than regularly spaced foils [11,12]. An analytic description of the TR spectrum generated in such radiators is, in general, not available. However, in some cases, a satisfactory approximation of some of the emission properties can be obtained by inserting the average values of spacing and membrane thickness into Eq. (3) for regular radiators [10].

3. Detector design principles

Many parameters affect the optimum design of a transition radiation detector system for a particular application. Among them are foil and gap material, foil and gap spacing, foil count, detector type, detector geometry, etc. Different applications require different optimizations, and often, the choice made for a parameter represents a compromise between competing requirements. In general, the design will be driven by the desired peak emission energy, ω_{peak}, and by the desired saturation Lorentz factor, γ_{sat}.

3.1. Radiator

The material of the radiator, be it composed of many foils or of fibers or foam, should be of high density and low atomic number. Therefore, solid hydrocarbons, such as polyethylene or Mylar, are suitable and practical materials. Low-Z metals, such as lithium or beryllium, would be very attractive, but are expensive and difficult to handle in practice [13].

The thickness of the foil (or the equivalent thickness of fibers or of foam membranes) is perhaps the most important detector parameter, because the characteristic TR emission energy, ω_{peak}, depends linearly on it (see Eq. (5)). As a general rule, if one wishes to observe TR from particles with relatively low Lorentz factors, one chooses small foil thicknesses, and consequently obtains relatively soft X-rays. For higher Lorentz factors, larger foil thicknesses are preferred, producing harder X-rays. The harder X-rays result from both an increase in ω_{peak}, and from more significant re-absorption of the softer X-rays in the thicker radiator foils.

Both the thickness of the foil and size of the gap help determine the saturation limit of a radiator. Increasing the gap size l_2 is expected to delay the onset of saturation effects, and push γ_{sat} higher (nominally, by the square root of the increase factor). However, a compromise must be found in practice, lest the length of the radiator become unreasonably large.

A radiator with fixed and constant values of l_1 and l_2 will allow an increase in the X-ray signal only over a limited range of Lorentz factors, generally covering less than one order of magnitude. If one wishes to extend this range, one can combine several radiator sections of differing properties into a single composite radiator stack. The parameters of each subsection in the stack are chosen to perform well within a specific, but different, range of Lorentz factors. However, the total response of such a composite radiator is not simply the sum of its components. This is due to a reduction in the X-ray yield by absorption in the downstream radiator materials. To ameliorate this effect, the upstream modules are best tuned to generate harder, more penetrating, X-rays than the

following modules, which are placed closer to the X-ray detectors.

3.2. Detector

Because of the small emission angles for TR photons, in most cases the X-rays are detected together with the ionization signal from the primary particle itself. Therefore, the X-ray detector should, in general, maximize photon absorption, while minimizing ionization by the particle. These conditions suggest a low-density, high-Z material: traditionally, xenon-filled proportional counters or chambers are used.

The atomic properties of the detector materials play an important role in the performance of a TRD. This is illustrated in Fig. 2, which shows a GEANT4 [14] simulation of the average energy deposit of X-rays in a 1 cm thick xenon layer at atmospheric pressure. As the figure shows, such a layer has near-100% collection efficiency for X-rays up to 6 keV. However, at higher energy, the X-rays are not always absorbed, and above 9 keV the average energy deposit begins to drop. The decline continues rapidly until roughly $\sim$35 keV, where the K-edge provides an increase in the photoelectric cross-section.

The increase in energy deposition at the K-edge makes it an attractive target at which to tune a radiator's peak emission energy. However, the total deposited energy may be less than expected because of the generation of fluorescence photons subsequent to a photoelectric interaction of the primary X-ray. These fluorescence photons will be on the low-energy side of the K-edge, and hence can easily escape from the detection volume. Therefore, only a portion of the primary X-ray energy will be collected.

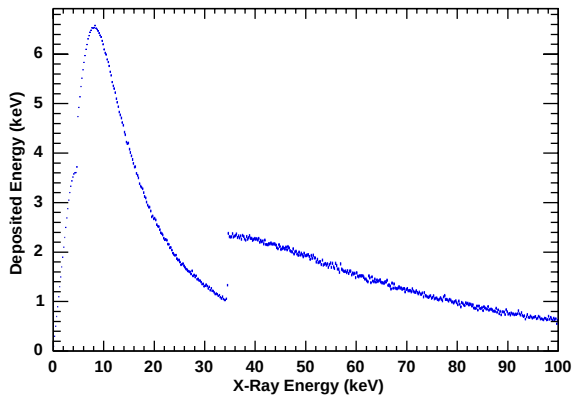

Fig. 2. GEANT4 simulation of the average energy deposit versus incident photon energy for a 1 cm chamber of xenon at 1 atm. The average includes those photons which deposit no energy in the detector volume.

For radiators with harder emission spectra, it is important to increase the efficiency for collecting the primary X-rays. This can be achieved by using a TRD which consists of a sandwich of multiple radiator/detector pairs. In this configuration, X-rays not absorbed in one detector are available as "feed-through" photons for possible collection in the downstream detectors. In some cases, it may also be useful to increase the thickness or the pressure of the xenon layer in order to increase the signal from the harder X-rays, even though the ionization signal of the particle will then also increase.

4. Measurements

The objective of the measurements described in the following was to determine whether a transition radiation detector can generate a measurable X-ray signal for particles with Lorentz factors as low as a few hundred without reaching saturation until $\gamma \sim 10^5$. Thus, this TRD should have a dynamic range of nearly three orders of magnitude for measurements of γ. We have designed the TRD according to the well-established precedent of placing xenon-filled proportional counters behind appropriately-chosen radiators. We have shown previously [12] that radiators with very thin foils or fibers are required to obtain TR response for γ-values less than one thousand. However, in order to push the saturation to values much beyond $\gamma \sim 10^4$, Eq. (6) indicates the need for radiators with relatively large values of l_1 and l_2. Thus, our requirements lead to a composite radiator which has both thin fibers for low-γ response, and thick foils for high-γ response.

The design of the high-γ radiator component proceeds as follows: because we use xenon as the detector gas, we tune the radiator such that the

highest peak in the frequency spectrum, ω_{peak}, is just above the K-edge in the absorption cross-section for X-rays in xenon. Hence, we chose Mylar foils with a nominal thickness of 3 mils ($l_1 = 76$ μm). With $\hbar\omega_1 \approx 24.4$ eV for Mylar, we then have $\hbar\omega_{peak} \approx \hbar l_1/2\pi c \approx 36.7$ keV. Eq. (6) for the saturation value γ_{sat} predicts $l_2 = 2.5$ cm for $\gamma_{sat} \sim 10^5$. As a practical radiator should exhibit at least ~ 100 interfaces (or 50 foils), this radiator would be over 1 m long. This is uncomfortably large for practical applications. Hence, the objective of our measurement is twofold: First, to ascertain whether a radiator designed along these lines can, indeed, reach a saturation level $\gamma_{sat} \sim 10^5$; and second, to investigate whether the length l_2 can be moderately reduced without seriously compromising the response.

To test the predictions, we carried out measurements at an external beam of the SPS at CERN/Geneva, using pions in the energy range from 20 to 350 GeV and electrons from 7 to 250 GeV. Signals were detected in 2-cm thick multiwire proportional chambers (MWPCs) filled with a xenon–methane (95–5%) mixture. The MWPCs had a wire spacing of 1 cm, and were installed in the beamline according to Fig. 3. These MWPC's have been used frequently by our group in the past (e.g., Ref. [12]), and are shown to be strictly proportional in response and uniform in gain across their area. The first chamber was placed upstream of all radiators in order to measure the specific ionization losses only. The other MWPCs were installed at fixed intervals behind it. Two upstream scintillator paddles served as a trigger, and their signals were used to select single-particle events.

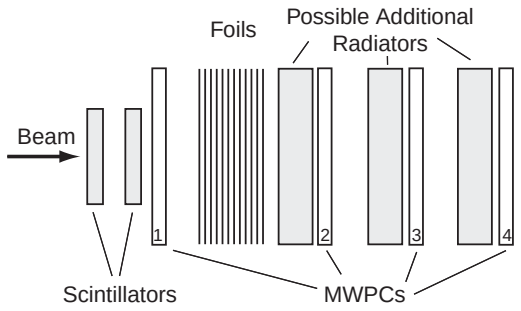

Fig. 3. Schematic view of the experimental set-up in the beam line.

In the base configuration, radiators with up to 51 Mylar foils at variable spacings l_2 could be placed in front of MWPC 2. The primary purpose of the additional downstream MWPCs was to study feed-through X-rays from the first radiator that were not absorbed in MWPC 2. Additional radiator materials could also optionally be placed in front of the last three chambers (see figure).

The signals from the MWPCs were read out with custom charge-integrating amplifiers (CSAs) and peak detectors. The peak levels were fed via a multiplexer into a flash-ADC system (Struck, SIS 3300). Four pairs of two adjacent wires per chamber were connected to each CSA. In the analysis, care was taken to only accept signals where the particle passed between the wires of a single pair by requiring that the adjacent wire pairs on either side showed zero signal.

For each radiator configuration, a background measurement was performed by replacing the radiators with solid blocks of plastic material of equivalent mass-density. Such a measurement would allow us to correct for background, such as bremsstrahlung contributions, to the measured signals, but such corrections were found to be negligible. Fig. 4 shows a typical pulse height distribution, measured with a radiator, and the corresponding background measurement.

The experimental configuration was simulated using the GEANT4 Monte Carlo package, version 5.2, patchlevel 1 [14]. Ionization losses

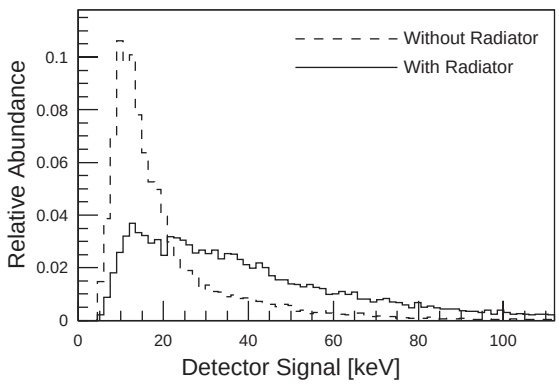

Fig. 4. Pulse-height distribution in a single MWPC with fiber radiators for 150 GeV electrons (solid histogram). The dashed histogram is obtained when the radiator is replaced by a solid plastic slab of an equivalent thickness.

were simulated using the G4hIonisation package, and transition radiation processes were simulated using both the G4GamDistrXTRdEdx and G4FoamXTRdEdx models, for multifoil and amorphous radiators, respectively [15]. The TR codes were slightly modified to operate beyond their default Lorentz factor upper limit of $\gamma \sim 10^5$. The TR photon energy limit was also increased by a factor of two, to 200 keV.

5. Results

We first investigate the response of the TRD for a single foil radiator volume as described above: we use 51 Mylar foils, 76 μm thick, spaced at $l_2 = 1.5$ cm. This value of l_2 is somewhat lower than indicated by Eq. (6) for saturation at $\gamma_{sat} \sim 10^5$ (see Section 2). Fig. 5 shows the average total signal (ionization loss of the particle plus TR) measured in chamber 2 for the Lorentz factor range $\gamma \sim 700$ to $\gamma \sim 3 \times 10^5$. Also shown are the signals in chamber 1 which are due only to ionization loss,

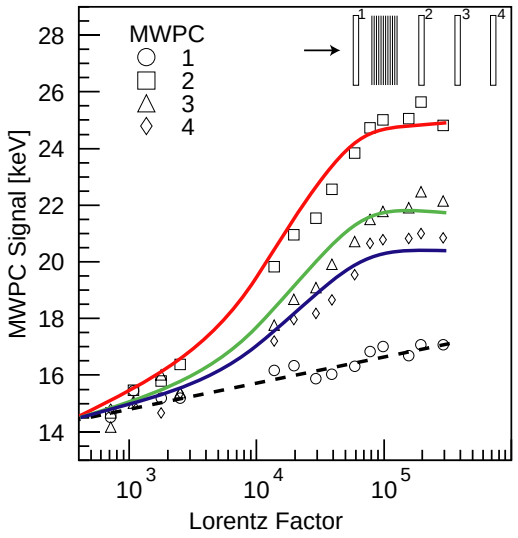

Fig. 5. Average detector signal versus Lorentz factor for 51 Mylar foils at 1.5 cm spacing. The foils were placed in front of chamber 2, as shown schematically in the upper right corner of the figure. The solid lines show the result of a GEANT4 simulation. The normalization to the data is arbitrary, but identical for all three lines. The dashed line indicates the trend of the chamber 1 data, measuring the ionization energy deposit.

and in chambers 3 and 4 which illustrate the feed-through of X-rays not detected in chamber 2. The solid lines indicate the results of the GEANT4 simulation; they have been arbitrarily normalized (by a single factor) to fit the data. There were no other radiators installed in this configuration.

The data in Fig. 5 establish that the foil radiator produce a signal which increases monotonically with Lorentz factor up to $\gamma_{sat} \sim 10^5$. Hence, this design makes possible, in principle, a measurement of γ up to these very high Lorentz factors. The data also show that the feed-through to subsequent chambers is significant, as can be expected for the production of relatively hard X-rays. The agreement of the data with simulations, at least in overall shape, and relative normalization, is quite satisfactory.

A drawback of the radiator used for the results in Fig. 5 is the large spacing between foils. For most practical applications, a more compact radiator with a smaller value of l_2 would be highly desirable. In order to investigate the response of the radiator as a function of l_2, we performed a number of measurements using again foils with $l_1 = 76$ μm, but varying the spacing, l_2.

Fig. 6a shows the measured yield at saturation (i.e., at $\gamma \sim 2 \times 10^5$), as a function of l_2. The yield here has been normalized by the specific energy deposit, at the same Lorentz factor. We note that, as predicted by the theory, the saturated yield does not vary significantly with the foil spacing over the range $l_2 = 0.5$–2 cm. From the same data, we have empirically determined a value of γ_{sat} for each spacing, l_2. Fig. 6b shows the result. Here we find that, at low spacings ($l_2 < 1.5$ cm), γ_{sat} appears to be systematically higher than the prediction of Eq. (6), shown as the dashed line. This unexpected result can have an important practical consequence: it indicates that a radiator somewhat more compact than that prescribed by Eq. (6) may be used without penalty in response at high Lorentz factors.

The response curve depicted in Fig. 5 illustrates a radiator that may be used for measurements of γ-values from about 10^4 to 10^5. If one wishes to extend the response to lower energies, one needs to add additional radiator materials. Previous measurements for the radiator combination used in the

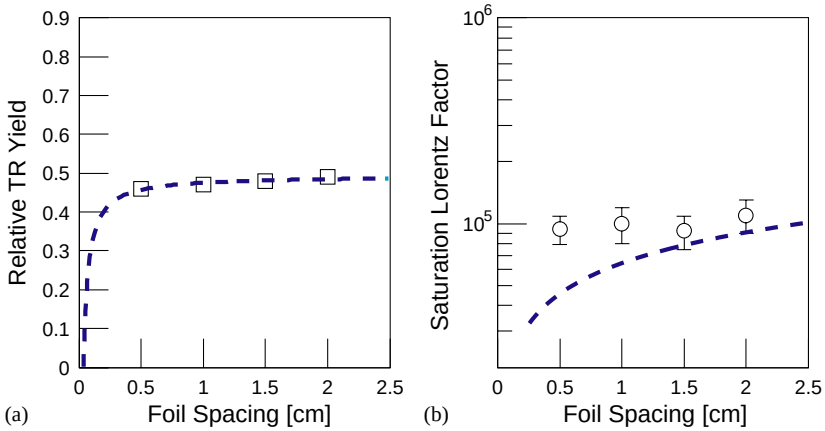

Fig. 6. Panel (a) shows the net TR yield (in units of the ionization signal measured in chamber 1) versus gap spacing for a Mylar foil radiator at $\gamma = 10^5$. Panel (b) shows the Lorentz factor of saturation, γ_{sat}, versus gap spacing for the same data. In both panels, the dashed lines indicate the calculated behavior. See text for details.

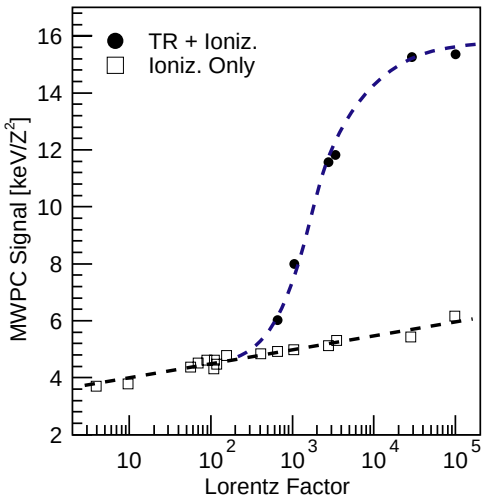

Fig. 7. Detector signal versus Lorentz factor from previous measurements of the CRN experiment [16], with (solid circles) and without (open squares) radiators in place. This figure includes singly-charged particles from accelerator calibrations, as well as nuclei from flight data. Note that in these measurements, 2 cm thick MWPCs with only 25% xenon content were used. The dashed lines serve to guide the eye.

CRN cosmic-ray detector [16] indicate how to proceed.

In that instrument, response at relatively low γ-values was achieved by using a combination of two kinds of plastic fiber radiators, a "thick" fiber of 17 μm and a "thin" fiber of 2–5 μm. Fig. 7 shows the response of the CRN radiator. With the exception of the data points above $\gamma = 10^4$, this response curve has been published previously [17]. We notice that for this radiator, TR begins to become observable at $\gamma \sim 500$, and may approach saturation above $\gamma \sim 10^4$.

The measurements for this figure were collected with a detector that employs only a rather small layer of xenon (2 cm thick gas mixture with 25% xenon content). It is instructive to investigate how the signals at high Lorentz factors might change if the xenon content is increased. Fig. 8 shows the response of the same radiator configuration, but now using a detector with 95% xenon in a 2 cm thick layer at 1 atm. Remarkably, a significant improvement in the signal over the Lorentz factor range $\gamma \sim 10^4$ to 10^5 can be observed, and the saturation is shifted to higher Lorentz factors. This is an interesting result which is not predicted by simulations that simply replace the fiber radiator with an equivalent combination of regularly spaced foils, nor by more sophisticated algorithms which try to take the irregularity of the radiator into account. It may be that the irregular fiber geometry leads to an enhancement in hard X-rays at high particle Lorentz factors which are then more efficiently absorbed in the increased xenon layer.

We now modify the foil radiator configuration by adding a fiber component, as discussed above.

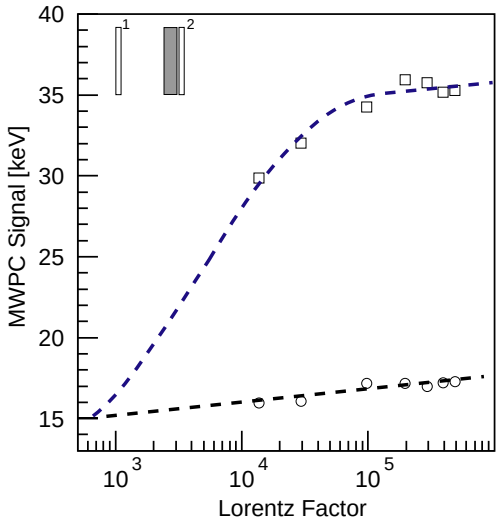

Fig. 8. Average detector signal versus Lorentz factor for a CRN-like radiator configuration. The open circles are data from MWPC 1, and the open squares are from MWPC 2, as shown in the inset schematic. The dashed lines serve to guide the eye.

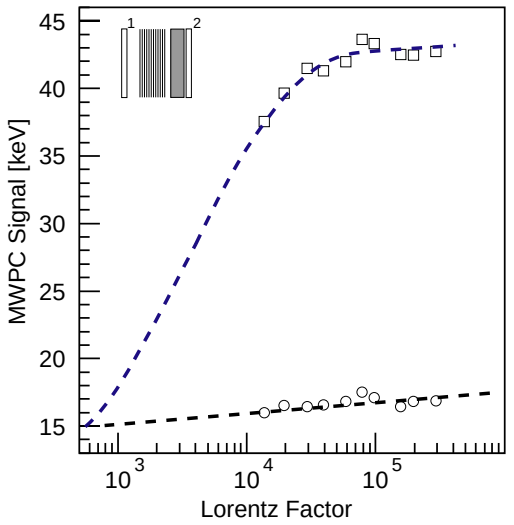

Fig. 9. Average detector signal for a radiator composed of 51 Mylar foils (spacing: 1.5 cm) and a CRN-type fiber radiator. Measurements are shown from MWPC 1 (open circles) and MWPC 2 (open squares), as defined in the inset schematic. The dashed lines indicate the trend of the data.

Fig. 9 shows the measured result: a further enhancement of the total response at high Lorentz factors. Importantly, the addition of new radiator material has not adversely affected the saturation limit. Although for this measurement, we were not able to obtain accelerator beams at γ values below 1000, it is reasonable to expect that, because of their common design features, the low-γ response will be similar to that shown in Fig. 7 for the CRN configuration. In contrast to the original design, however, the new combination exhibits a response that extends to much higher values of γ.

In another set of tests, we use a somewhat modified configuration, replacing some of the fibers of the CRN radiator with a 5 cm block of DOW Ethafoam 220, a closed-cell, polyethylene foam with a density of 36 g/l. The results are illustrated in Fig. 10. Again, an unsaturated response that reaches up to Lorentz factors of $\gamma \sim 10^5$ is seen. For comparison, Fig. 10 also shows the results obtained with a single foil radiator as given in Fig. 5. Again, the addition of extra radiator materials to the foil stack increases the overall yield without serious detriment to the saturation point, γ_{sat}.

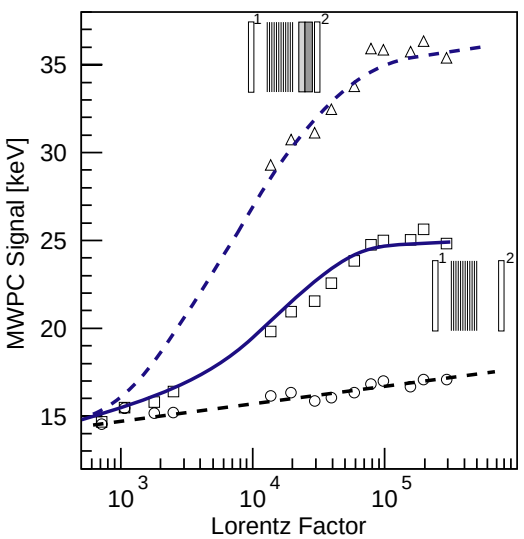

Fig. 10. Average detector signal versus Lorentz factor for two radiator configurations (see inset schematics). The open triangles show data from MWPC 2 for a radiator with 51 Mylar foils (spacing: 1.5 cm), 5 cm of Ethafoam, and 7.6 cm of 17 μm fibers ($\rho = 40$ mg/cm^3. Also shown is the response from the foils alone (open squares, see Fig. 5), and from MWPC 1 (open circles). The dashed lines indicate the trend of the data, and the solid line shows the result of a GEANT4 simulation.

6. Discussion

The measurements described here demonstrate that it is possible to construct practical transition radiation detectors that show a γ-dependent response up to Lorentz factors of $\gamma \sim 10^5$. Furthermore, when combined with previous measurements of low-γ TRDs, they indicate that it is possible to simultaneously achieve, in the same detector, sensitivity for Lorentz factors near $\gamma \sim 500$. This result is of great importance for the design of detectors for heavy cosmic-ray nuclei. Such detectors will permit detailed studies of the cosmic-ray composition and energy spectra of individual elements up to energies around 10^{15} eV per particle.

It appears that transition radiation theory, and the simulations built upon it, are capable of predicting the behavior of a TRD quite well for regular foil radiators. For random foam and fiber materials, calculations using the average material thicknesses and spacings give qualitative guidance for predicting their behavior. However, it appears that such calculations may underestimate the observable signals near saturation. This is a result of considerable practical importance. Another gratifying result of the measurements is the fact that the l_2-dependence of the transition radiation yield at saturation is not very strong, making possible the construction of foil radiators that are more compact than expected on the basis of previous estimates.

It is clear that further tuning of the parameters of the radiator/detector configuration could lead to additional improvements in response. Although simulations based on theory give some guidance, such optimization efforts may not be reliable unless they are verified by calibrations at accelerator beams.

Acknowledgements

The authors gratefully acknowledge the technical assistance of P. Barbeau, E. Drag, G. Kelderhouse, and R. Northrop at Chicago and N. Bechtold, H. Bolz, W. Paulus, and M. Riegel from Forschungszentrum Karlsruhe. This work was supported, in part, by NASA grants NAG5-5072 and NAG5-5305. F.G. acknowledges support from the Aerospace Illinois Space Grant.

References

[1] V.L. Ginzburg, I.M. Frank, Zh. Eksp. Teor. Fiz. 16 (1946) 15.
[2] C. Favuzzi, N. Giglietto, M.N. Mazziotta, P. Spinelli, Riv. Nuovo Cim. 24N5-6 (2001) 1.
[3] S.P. Wakely, Astropart. Phys. 18 (2002) 67.
[4] S.P. Swordy, et al., Astropart. Phys. 18 (2002) 129.
[5] G.M. Garibian, Sov. Phys. JETP 10 (1960) 372.
[6] G.M. Garibian, Sov. Phys. JETP 33 (1971) 23.
[7] M. Ter-Mikaelian, Effect of the Medium on Electromagnetic Processes at High Energies, AN ArmSSR, 1969.
[8] M.L. Cherry, et al., Phys. Rev. D 10 (1974) 3594.
[9] X. Artru, G.B. Yodh, G. Mennessier, Phys. Rev. D 12 (1975) 1289.
[10] M.L. Cherry, Phys. Rev. D 17 (1978) 2245.
[11] T.A. Prince, et al., Nucl. Instr. and Meth. 123 (1975) 231.
[12] S.P. Swordy, J. L'Heureux, D. Muller, P. Meyer, Nucl. Instr. and Meth. 193 (1982) 591.
[13] J. Cobb, et al., Nucl. Instr. and Meth. 140 (1977) 413.
[14] S. Agostinelli, et al., Nucl. Instr. and Meth. A 506 (2003) 250.
[15] J. Apostolakis, S. Giani, M. Maire, A.V. Bagulya, V.M. Grichine, Comput. Phys. Comm. 132 (2000) 244.
[16] J. L'Heureux, J.M. Grunsfeld, P. Meyer, D. Muller, S.P. Swordy, Nucl. Instr. and Meth. A 295 (1990) 246.
[17] S.P. Swordy, et al., Phys. Rev. D 42 (1990) 3197.